Journal of
Synchrotron
Radiation

ISSN 1600-5775

Received 29 April 2013
Accepted 17 September 2013

Influence of co-dopant in the europium reduction in $SrAl_2O_4$ host

Marcos V. dos S. Rezende,[a]* Paulo J. R. Montes,[b] Felipe M. dos S. Soares,[c] Claudiane dos Santos[c] and Mário E. G. Valerio[c]

[a]Instituto Federal de Sergipe, Aracaju, SE 49055-260, Brazil, [b]Instituto Federal de Sergipe-IFS, Largato, SE 49400-000, Brazil, and [c]Departamento de Física, Universidade Federal de Sergipe, Campus Universitário, São Cristovão, SE 49100-000, Brazil. *E-mail: mvsrezende@gmail.com

Xerogels of strontium chlorate and aluminium chlorate doped with europium (un-co-doped) and co-doped with rare earth ions (Ln = Gd, Dy, Er and Y) were prepared using the proteic sol–gel route. Synchrotron radiation was used to investigate the effect of different co-dopants on the $Eu^{3+} \rightarrow Eu^{2+}$ reduction process during the synthesis of the samples. Samples were excited at the Eu L_{III}-edge and the XANES regions were analyzed. The results suggest that some of the Eu ions can be stabilized in the divalent state and that it is difficult to completely reduce Eu^{3+} to Eu^{2+} during thermal treatment. The mechanisms of the Eu reduction processes are explained by a proposed model based on the incorporation of charge-compensation defects.

Keywords: europium reduction; DXAS measurements; defects.

1. Introduction

Strontium-aluminate-based phosphors have been extensively investigated owing to their persistent phosphorescence with a high quantum efficiency and good chemical stability (Lu & Shu, 2007; Yokota *et al.*, 2001; Ravichandran *et al.*, 1997; Ellens *et al.*, 2001). These properties occur when the strontium aluminate phosphors are activated by Eu^{2+} ions and are finding use in a variety of applications such as luminous paints, emergency lighting, safe traffic, wall painting, films, artificial fibres, rubbers, textiles ceramics, lamp industry, colour display, radiation dosimetry, X-ray imaging, *etc.* (Clabau *et al.*, 2005).

The activated Eu^{2+} ions are normally obtained *via* reduction of Eu^{3+} to Eu^{2+} during sample annealing, since trivalent europium oxide, Eu_2O_3, is usually the starting material used for doping. Thus, the phosphors are generally prepared under an atmosphere that contains a reducing agent during annealing (Takeyama *et al.*, 2004; Montes & Valerio, 2010; Dorenbos, 2005*a*,*b*; Zhang *et al.*, 2002; Peng *et al.*, 2003). In some compounds, a material containing Eu^{3+} ions can be easily reduced to the Eu^{2+} valence state in a reducing atmosphere. In other cases, it is difficult to obtain the Eu^{2+} ion when the sample is prepared using a gas as the reducing atmosphere (Pei *et al.*, 1996). In a few compounds, the reduction of Eu^{3+} to Eu^{2+} can occur when samples are annealed in air at high temperature (Zeng *et al.*, 1998; Peng *et al.*, 2003).

The duration of long-lasting phosphorescence emission can be increased by co-doping with rare earth ions, especially Dy^{3+} ions (Clabau *et al.*, 2005). Many studies have been dedicated to understanding the relationship between Dy^{3+} ions and hole traps. However, this relationship is still not fully understood. Some studies proposed that the Dy^{3+} ion traps a hole (*e.g.* Matsuzawa *et al.*, 1996), while others proposed that the Dy^{3+} ions induce the formation of hole traps associated with a charge-compensating defect (*e.g.* Ohta *et al.*, 2000). Therefore, important questions remain with respect to the reduction mechanism and further investigation is needed. Knowing the effect of rare earth (3+) ions, such as Gd, Dy, Er and Y, as co-dopants can help to clarify the trapping mechanism of the charge carriers and their effects on the phosphorescent process of Eu-doped $SrAl_2O_4$.

Previous X-ray absorption spectroscopy (XAS) measurements have been used to study valence states in persistent phosphors such as $SrAl_2O_4$:Eu,Dy (Korthout *et al.*, 2011), and the valence changes of lanthanide ions were observed in other systems in real time using XAS (Korthout *et al.*, 2013). These authors studied the valence state changes of europium in Ca_2SiS_4, and Moreau *et al.* (2002*a*,*b*) have investigated the valence state changes of europium in aqueous and non-aqueous systems upon exposure to oxygen. Martin *et al.* (1980) recorded the valence state changes of samarium in $Sm_{0.75}Y_{0.25}S$ upon heating.

In the present work, the effect of the Ln^{3+} (Ln = Gd, Dy, Er or Y) co-dopant ions on the reduction of the Eu^{3+} ions was followed *in situ*. X-ray absorption near-edge structure (XANES) measurements around the Eu L_{III}-edge in $SrO:Al_2O_3:Eu,Ln$ were carried out using H_2-containing atmospheres as the reduction agent. In order to be able to follow the valence changes during the entire thermal program, the XANES spectra were recorded using the dispersive X-ray absorption spectroscopy (DXAS) beamline at the LNLS (Brazilian Synchrotron Light Laboratory). The measurements

were used to propose a mechanism for the Eu reduction and stabilization within the samples.

2. Experimental

Samples doped with 2.0 mol% of Eu and co-doped with 1.0 mol% of Ln (Ln = Dy, Er, Y, Gd) were prepared *via* a proteic sol–gel route (Macedo & Sasaki, 2002) with stoichiometric mixtures consisting of $SrCl_2{\cdot}6H_2O$, $AlCl_3{\cdot}6H_2O$ and $EuCl_3{\cdot}6H_2O$ in coconut water (*Cocos nucifera*). The samples evaluated in these experiments were pre-calcined at 873 K for 1 h in open air in order to eliminate adsorbed water and part of the organic material from the coconut water present in the xerogel. The pre-calcined xerogels were fired under a reduction atmosphere (5%H_2 + 95%He) in a furnace and the reduction of the samples was carried out *in situ* during the XANES measurements, as described below.

XANES measurements were performed at the DXAS beamline at the National Synchrotron Light Laboratory (LNLS) in Brazil (Rodrigues *et al.*, 1998). A polychromatic X-ray beam with bandpass close to the Eu L_{III}-edge region (around 6977 eV) was selected using a curved Si(111) crystal and the beam was focused down to a few micrometres in the sample (Cezar *et al.*, 2010). The X-ray beam passing through the sample was collected on a CCD detector and a full XANES spectrum can be collected every few tenths or hundredths of a millisecond, depending on the intensity of the XANES signal being measured. This dispersive arrangement allows fast data acquisition and kinetic X-ray absorption measurements can be carried out. In the present work, spectra were recorded as a function of the temperature of the sample in order to check the change in the position of the absorption edge of the Eu dopants that corresponds to changes in the oxidation state of the Eu cations. The samples were mixed with BN powders and pellets of ~10 mm diameter and ~1 mm thickness were obtained. The mixing with BN is important to obtain a self-sustaining pellet that can be held in a sample holder inside the furnace. The furnace is composed of a quartz tube, with water-cooled Kapton windows installed at either end, inside a heating element. The desired atmosphere was streamed through during the experiment and a type-K thermocouple, installed inside the furnace very close to the sample, was used to measure the sample temperature. The samples were submitted to a temperature program which can be divided into three parts: (i) a heating stage, following a heating rate of 10 K min^{-1} from room temperature to 1373 K. This was found to be the best condition for the formation of $SrAl_2O_4$ in a previous work (Montes & Valerio, 2010); (ii) a setting stage, that consists of keeping the sample at 1373 K for a duration of 60 min; (iii) a cooling stage, that consists of cooling down the sample to room temperature following a cooling rate of -10 K min^{-1}. During all three stages XANES spectra were collected continuously. Standard Eu_2O_3 was also measured at room temperature in the same experimental set-up and was used to compare the Eu-edge position and also to calibrate the pixels of the CCD detector. The pixel calibration was made by comparing the XANES curves of the Eu_2O_3 measured at the DXAS beamline with a measurement of the same sample carried out at the XAFS2 beamline of the LNLS, which is a conventional monochromatic X-ray absorption beamline.

3. Results

Fig. 1(*a*) shows a selected sequence of XANES spectra measured around the Eu L_{III} absorption edge of the pre-calcined xerogel ($SrO{:}Al_2O_3$:Eu, un-co-doped) as a function of temperature. The xerogel begins to decompose and subsequent reactions lead to the formation of $SrAl_2O_4$. The Eu L_{III} XANES spectra have a strong absorption line at the absorption edge due to $2p^{3/2} \rightarrow 5d$ electronic transitions. The XANES spectra of the standard sample of Eu_2O_3, taken in the same arrangement, are also shown in Fig. 1(*a*). This comparison is used as a reference for the Eu^{3+} absorption edge. The first thing that can be noticed is that the signal-to-noise ratio is much worse for the Eu-doped samples than for the standard sample. There are three main reasons for this: (i) the Eu concentration in the reference sample is obviously much higher than in the doped samples, (ii) the XANES spectra were collected in transmission mode and this mode is not particularly appropriate for measuring samples with a low concentration, and (iii) the XANES measurements were made during the formation of the sample upon heating and most of the starting mass is lost due to the reactions that form the $SrAl_2O_4$ crystalline phase from the xerogel. This last reason is the most significant factor for measurements taken at high temperatures, since the sample mass decreases as the temperature increases. This feature was also noted when the samples were removed from the furnace. The thickness of the sample was lower than the thickness of the starting pellet and this depends on the amount of BN added to the pellets. In some of the samples holes were formed. The results presented here were taken for pellets where the sample itself was reduced in thickness but no hole was observed after calcination. The overall effect is that the X-ray beam was transmitted through a sample layer which became thinner as the temperature increased. As a consequence, a decrease in the absorption jump is seen in the spectra, increasing the signal-to-noise ratio.

In the first spectrum, taken at room temperature [spectrum marked as '298 K-heating' in Fig. 1(*a*)], the presence of Eu^{3+} ions is evident from the comparison with the Eu_2O_3 reference spectrum [also shown in Fig. 1(*a*)]. Upon increasing the temperature, two well resolved resonance lines, corresponding to two different absorption edges, are visible. These can be associated with the presence of two valence states for the Eu ions. The divalent and trivalent valence states can be easily distinguished because their absorption edges are quite different. The absorption edge for Eu^{2+} is approximately 8 eV below the Eu^{3+} edge, which is compatible with the reference compounds of Eu^{2+} and Eu^{3+} (Wortmann, 1989). The reason for this energy difference is the lower binding energy of the core electrons in Eu^{2+} caused by the shielding of the nucleus by the additional 4*f* electron. As the oxidation state increases,

it is a well known behaviour that the energy to remove an electron from the ion core also increases (Korthout *et al.*, 2011, 2013; Moreau *et al.*, 2002*a*). This effect can be understood by considering that the remaining electrons in the ion become more tightly bound to the ion core due to an increase in the net positive charge and also to a reduction of the ionic radius. Moreover, the electron–electron repulsion decreases and this additional effect helps to decrease the ionic radius and, as a consequence, increases the binding energies of the core electrons.

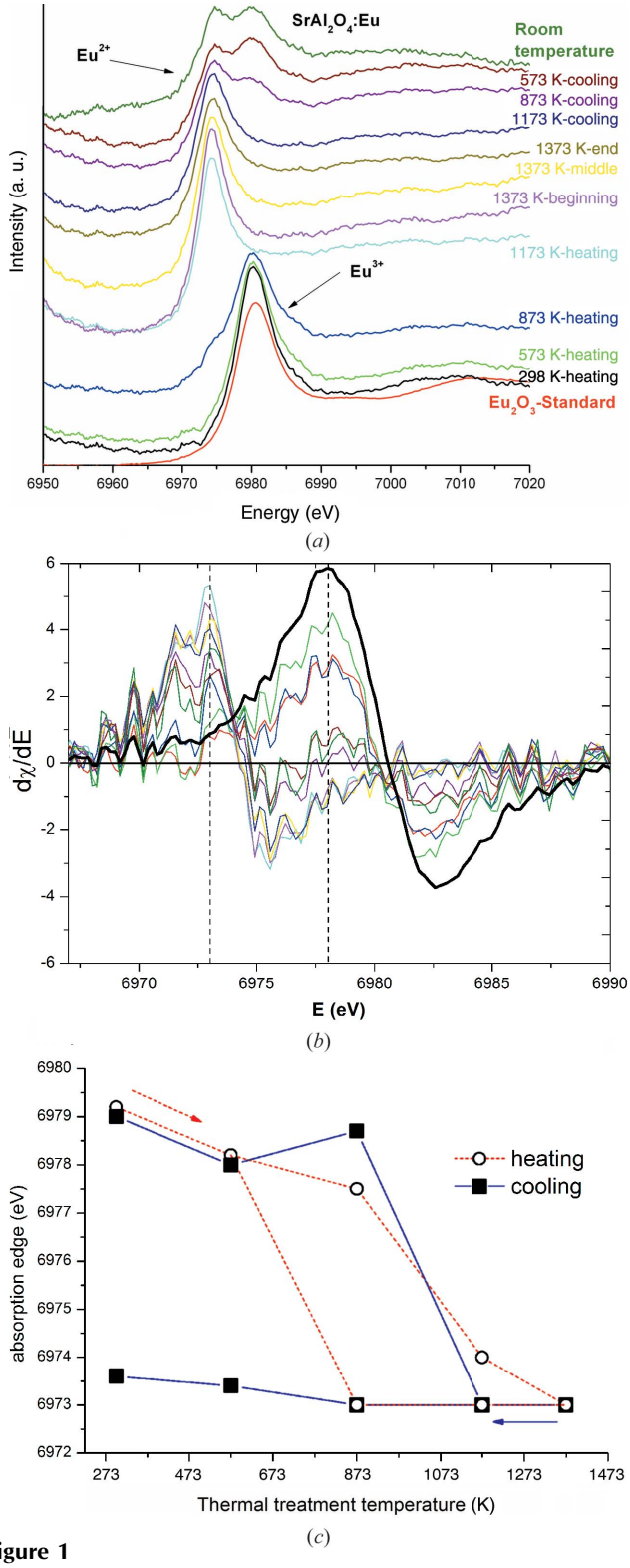

Figure 1
Sequence of XANES spectra of pre-calcined xerogel doped with Eu as a function of temperature.

The presence of two absorption edges is an indication that Eu^{3+} ions are reduced to Eu^{2+} ions due to the annealing process in the H_2/N_2 atmosphere. Fig. 1(*b*) displays the dependence of the derivative of the absorption curves ($d\chi/dE$) as a function of the energy for different temperatures in the calcination program. The maxima in the derivative curves indicate the inflexion points that can be assigned to the absorption edges of the chemical species. The thermal evolution of the ($d\chi/dE$) maxima shows that two maxima can be identified around 6973 and 6978 eV, associated with the Eu^{2+} and Eu^{3+} species, respectively. The evolution of these two maxima as the thermal program proceeds can be seen in Fig. 1(*c*). At room temperature the xerogel exhibits only the trivalent species indicated by the presence of one maximum in the curve. This maximum is slightly shifted to a lower energy when the temperature reaches 573 K, indicating that a small amount of Eu^{2+} has already been formed. At 873 K, the ($d\chi/dE$) curve clearly exhibits two maxima indicating that both species are already present and these two maxima stay up to the middle of the setting stage when the two maxima are reduced to just one in the position of the Eu^{2+} absorption edge. Upon cooling, both species are again visible and, at the end of the process, the $SrAl_2O_4$ sample formed has both Eu^{2+} and Eu^{3+} species since two maxima are observed in the respective energies.

These results suggest that the Eu^{2+} state is more stable in hexagonal phases (stable at high temperature) than monoclinic phases (stable at low temperature) since the phase transition between the two phases was found to be at around 923 K. These results also suggest that not all Eu added to the sample is actually converted to the desired divalent state upon heating treatment in a reducing atmosphere. The amount of Eu^{2+} and Eu^{3+} remaining in the sample is not easily obtained from this set of measurements because, as discussed earlier, the XANES signals are quite noisy and any model that could be fitted to the data will be susceptible to a high degree of uncertainty.

Figs. 2, 3, 4 and 5 show similar annealing cycles for the Eu-doped pre-calcined xerogels, but now the samples are co-doped with Gd, Dy, Er and Y ions, respectively. In all cases, upon increasing the temperature in the annealing process, two well resolved edges are visible, indicating two valence states for the Eu ions. At 1173 K or higher, the XANES spectra are dominated by the Eu^{2+} absorption edge peak. In the cooling step, it is observed that the absorption peak related to Eu^{2+} decreases and the one for Eu^{3+} increases, which is consistent with the return of some of the Eu^{2+} to the trivalent state. The only difference, observed for samples with different co-dopants, is related to the relative intensity of the absorption edge due to Eu^{2+} and Eu^{3+} after the heating cycle, *i.e.* the ratio $[Eu^{2+}]/[Eu^{3+}]$, although it was not very easy to quantify this. The results suggest that the presence of the different co-

dopants induced different amounts of the Eu^{2+} ion after the heating cycle.

Katsumata *et al.* (2006) studied the photoluminescence spectra from $SrAl_2O_4$:Eu,Ln (Ln = La, Ce, Pr, Nd, Sm, Gd, Tb, Dy, Ho, Er, Tm, Yb, Lu and Y) samples. They reported three main influences of the co-dopant ions. Firstly, they found that the emission peak maximum associated with the 5*d*–4*f* transition of the Eu^{2+} ions did not change for different co-dopants. This implies that the crystal field of the Eu^{2+} ions did not change significantly with the presence of the co-dopant. Secondly, they observed that the emission intensity of the Eu^{2+} ions depends strongly on the co-dopant ions. Thirdly, the trap depth (or the thermal activation energies of the traps) and the densities of the trapped carriers are dependent on the co-dopant ions. According to Dorenbos (2005*b*), the photo-generated electron would be trapped at Ln^{3+} sites thereby reducing Ln^{3+} to Ln^{2+}. Clabau *et al.* (2005, 2006), on the other hand, proposed an alternative mechanism explaining the effect of the co-dopant on the phosphorescence decay time. Their model is based on the stabilization of the 'pre-existing' electron traps caused by the presence of interactions between dopant (co-dopant) cations and oxygen vacancies.

From the present work, it can be seen that the co-dopant ion can also influence the $[Eu^{2+}]/[Eu^{3+}]$ ratio obtained after the reduction process. This information is important, since the Eu^{2+} ions are responsible for the main long-lasting emission in $SrAl_2O_4$ and were also found to be an important factor for the long phosphorescence in the model proposed by Clabau *et al.* (2005, 2007).

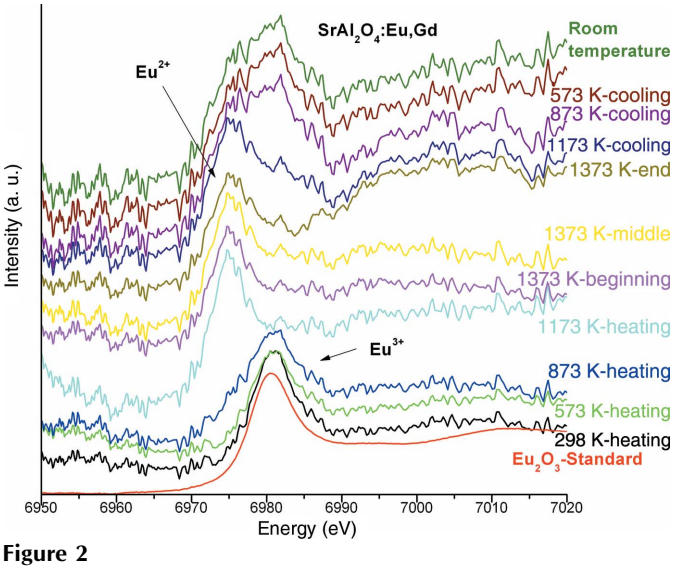

Figure 2
Sequence of XANES spectra of the pre-calcined xerogel doped with Eu and Gd as a function of temperature.

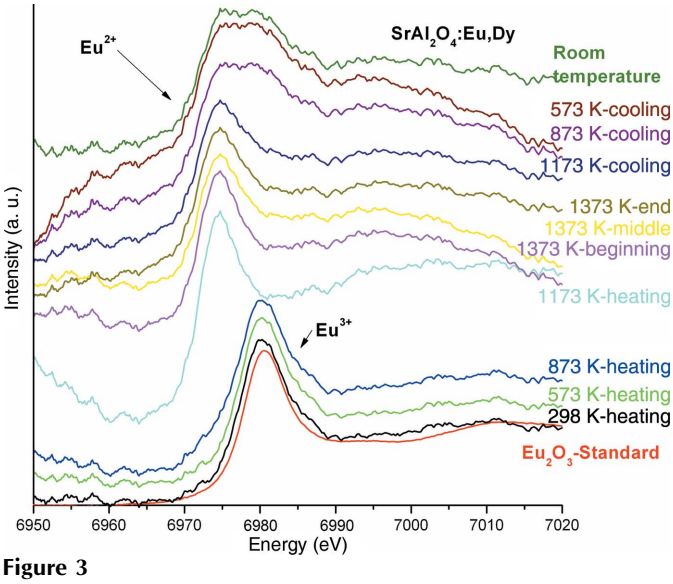

Figure 3
Sequence of XANES spectra of strontium aluminate, doped with Eu pre-calcined xerogel and co-doped with Dy ions, as a function of temperature.

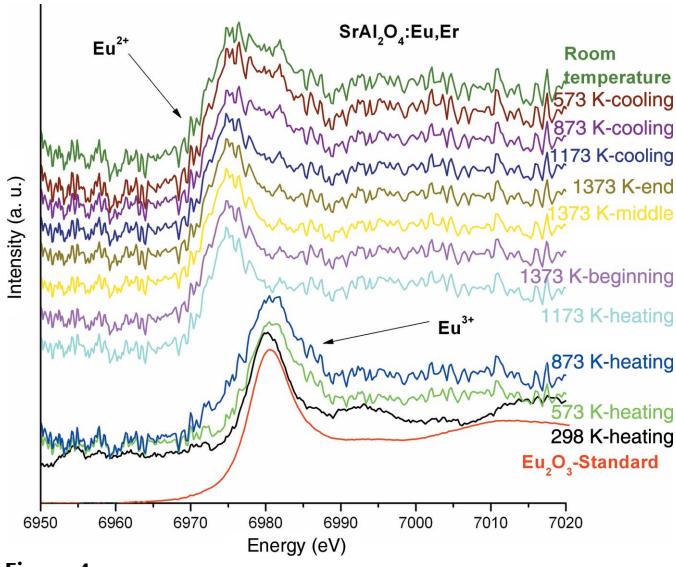

Figure 4
Sequence of XANES spectra of strontium aluminate, doped with Eu pre-calcined xerogel co-doped with Er ions, as a function of temperature.

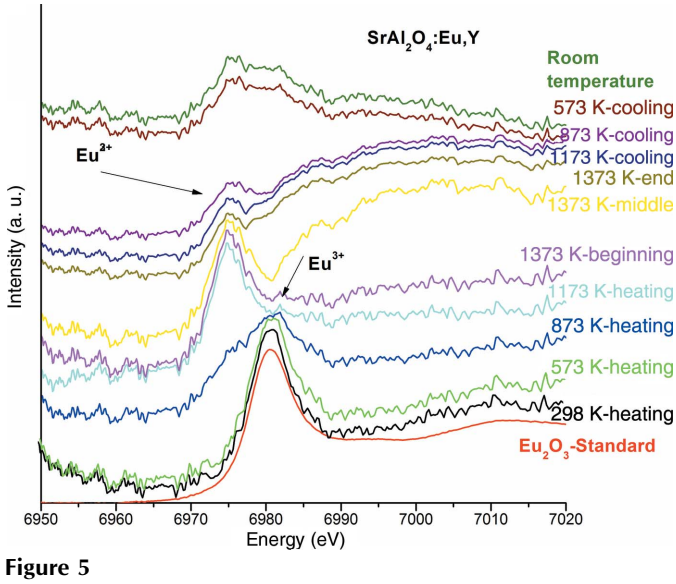

Figure 5
Sequence of XANES spectra of strontium aluminate, doped with Eu pre-calcined xerogel co-doped with Y ions, as a function of temperature.

None of the above models explain how the two valences are actually accommodated inside the $SrAl_2O_4$ matrix and, in the case of the trivalent species, which are the charge-compensating defects. Moreover, since during the annealing under a reducing atmosphere the Eu valence state changes from 3+ to 2+, what happens to the charge-compensating defects and what is the role played by the atmosphere in the process? The results presented herein can be used as a starting point to propose a model for the entire process. The annealing cycles will be divided into three stages: stage (i), at the beginning of the heating cycle, when the XANES spectra are dominated by Eu^{3+} ions; stage (ii), the high-temperature part of the heating cycle, when the XANES spectra are dominated by Eu^{2+} ions; stage (iii), the final part of the cycle, comprising the cooling down to room temperature, when some of the Eu^{2+} ions are converted back to the trivalent state.

In stage (i), the substitution of Eu^{3+} at the Sr^{2+} site, $Eu_{Sr}^{\bullet}$ (a single subscript $\bullet$ indicates a single positive charge; Kroger & Vink, 1954), is an aliovalent substitution requiring that some charge-compensating defects must be formed to keep the neutrality of charges throughout the sample. Previous computer modelling results (Rezende *et al.*, 2012) revealed that the main charge-compensating defect is interstitial oxygen (using Kroger–Vink notation, O_i'') located near the Eu^{3+} ions. The reaction corresponding to the defect formed in this stage is given by equation (1), where Kroger–Vink notation is used to represent the defects,

$$Eu_2O_3 + 2Sr_{Sr} \rightarrow (2Eu_{Sr}^{\bullet} + O_i'') + 2SrO. \quad (1)$$

In stage (ii), the following mechanism can be suggested. The high temperature causes breakdown in some of the H_2 molecules in the surrounding atmosphere, forming free H atoms that can react with the sample. Two types of defects can be proposed that may act as electron donors to the reduction of the Eu ions. The first one is the reaction of an atomic H atom with the O_i'', already present in the sample, to give a OH_i' defect. The electron lost by the H^+ ion to react with the interstitial oxygen ion is transferred to the Eu^{3+} ion forming the Eu^{2+} one. The second mechanism is the reaction of the two free atomic H atoms with interstitial oxygen ions which form water vapour (H_2O) that is lost by the sample. Then, the two electrons left behind by the O_i'' are used to reduce the Eu^{3+} ions. As a result, some of the Eu^{3+} ions are reduced to Eu^{2+}. Both proposed mechanisms involve the participation of the O_i'', that is largely formed due to the presence of the Eu^{3+}, as the charge-compensating defect. This means that the reactions that took place between the atomic H from the atmosphere and the O_i'' happened very close to the Eu^{3+} ions, increasing the possibility of the free electrons transferring to the Eu ions. These processes that happen in stage (ii) can be represented by the following equations,

$$2Eu_{Sr}^{\bullet} + O_i'' + 2SrO + \tfrac{1}{2}H_2 \rightarrow (\underbrace{Eu_{Sr}^{\bullet} + OH_i'}_{Eu^{3+}} + \underbrace{Eu_{Sr}^{\times}}_{Eu^{2+}}) + 2SrO, \quad (2)$$

$$2Eu_{Sr}^{\bullet} + O_i'' + 2SrO + H_2 \rightarrow (\underbrace{2Eu_{Sr}^{\times}}_{Eu^{2+}}) + 2SrO + H_2O. \quad (3)$$

Equations (2) and (3) describe the reactions involving the reduction of the Eu^{3+} ions due to the incorporation of free H atoms in the sample with generating, as sub-products, either OH^- [equation (2)] or water vapour [equation (3)]. Both processes may happen at the same time as the temperature changes. The important difference between them is that the process forming OH^-, and described by equation (2), can be reversible if the sample loses atomic H at the same time as the Eu^{2+} loses the extra electron to the O_i. The process involving the production of water vapour, on the other hand, cannot be reversed because the water molecule lost by the sample was washed out by the H_2/He flux inside the furnace. These features can be used to explain what happens in stage (iii).

Stage (iii) is basically a partially reversible process where some of the Eu^{2+} ions return back to their original trivalent state. If the discussion in the preceding paragraph is taken into account, added to the fact that the OH^- defect was found to be an unstable defect in some oxide compounds (Filip *et al.*, 2006; Lengyel *et al.*, 2010), it is possible to postulate that, while the mechanism described by equation (3) can be associated with the Eu^{2+} remaining in the sample at room temperature during the cooling down cycle, the mechanism described by equation (2) involving OH^- defects inside the sample is responsible for the amount of Eu^{2+} that was reoxidized to the trivalent state due to the release of captured, at high temperature, H atoms.

The results of the thermal cycle for the co-doped samples, as already discussed, indicate that the co-dopants play an important role in the stabilization of either of the Eu valences in the samples. According to the qualitative model described above, it is possible to say that the effect of the co-dopant is to change the relative Gibbs free energy of the mechanisms described by reactions (2) and (3) in a way that either the formation of OH^- defects or the loss of water vapour by the sample is the most favourable one. By changing the relative Gibbs free energies of the reactions, the co-dopants will induce the stabilization of larger quantities of Eu^{2+} in the sample or the reversibility of the entire process.

4. Conclusions

The influence of a co-dopant ion on the stabilization of Eu^{2+} ions in strontium aluminates produced by the proteic sol–gel route was investigated using DXAS measurements as a function of temperature in a 5%H_2/95%He atmosphere. The results suggested that some of the total Eu ions can be stabilized at the divalent state and that it is not universally possible to reduce all Eu^{3+} to Eu^{2+} after a thermal treatment. During the heating cycle, it was observed that the XANES spectra are dominated by an Eu^{2+} absorption edge peak at high temperature. But, upon cooling, the process is partially reversible. It was also observed that the co-dopant ion can also influence the $[Eu^{2+}]/[Eu^{3+}]$ ratio, after the reduction treatment. The Eu reduction processes are explained by a

proposed model based on two mechanisms involving the reaction of free atomic H atoms with the charge-compensating defects producing, as sub-products, either OH^- inside the sample or water vapour.

The authors are grateful to FINEP, CAPES, INAMI, CNPq and LNLS for financial support. Research was supported by the LNLS (Brazilian Synchrotron Light Laboratory)/MCT project DXAS No. 11862/11.

References

Cezar, J. C., Souza-Neto, N. M., Piamonteze, C., Tamura, E., Garcia, F., Carvalho, E. J., Neueschwander, R. T., Ramos, A. Y., Tolentino, H. C. N., Caneiro, A., Massa, N. E., Martinez-Lope, M. J., Alonso, J. A. & Itié, J.-P. (2010). *J. Synchrotron Rad.* **17**, 93–102.
Clabau, F., Rocquefelte, X., Jobic, S., Deniard, P., Whangbo, M., Garcia, A. & Le Mercier, T. (2005). *Chem. Mater.* **17**, 3904–3912.
Clabau, F., Rocquefelte, X., Jobic, S., Deniard, P., Whangbo, M., Garcia, A. & Le Mercier, T. (2007). *Solid State Sci.* **9**, 608–612.
Clabau, F., Rocquefelte, X., Le Mercier, T., Deniard, P., Jobic, S. & Whangbo, M. (2006). *Chem. Mater.* **18**, 3212–3220.
Dorenbos, P. (2005*a*). *Chem. Mater.* **17**, 6452–6456.
Dorenbos, P. (2005*b*). *J. Electrochem. Soc.* **152**, h107.
Ellens, A., Zwaschka, F., Kummer, F., Meijerink, A., Raukas, M. & Mishra, K. (2001). *J. Lumin.* **93**, 147–153.
Filip, J., Novák, M., Beran, A. & Zboril, R. (2006). *Phys. Chem. Miner.* **32**, 733–746.
Katsumata, T., Toyomane, S., Sakai, R., Komuro, S. & Morikawa, T. (2006). *J. Am. Ceram. Soc.* **89**, 932–936.
Korthout, K., Parmentier, A. B., Smet, P. F. & Poelman, D. (2013). *Phys. Chem. Chem. Phys.* **15**, 8678–8683.
Korthout, K, Van den Eeckhout, K., Botterman, J., Nikitenko, S., Poelman, D. & Smet, P. F. (2011). *Phys. Rev. B*, **84**, 085140.
Kroger, F. A. & Vink, H. J. (1954). *J. Chem. Phys.* **22**, 250.
Lengyel, K., Timón, V., Hernández-Laguna, A., Szalay, V. & Kovács, L. (2010). *IOP Conf. Ser. Mater. Sci. Eng.* **15**, 012015.
Lu, W. & Shu, X. (2007). *Rare Metals*, **26**, 305.
Macedo, M. A. & Sasaki, J. M. (2002). Patent INPI 0203876-5.
Martin, R. M., Boyce, J. B., Allen, J. W. & Holtzberg, F. (1980). *Phys. Rev. Lett.* **44**, 1275–1278.
Matsuzawa, T., Aoki, Y., Takeuchi, N. & Murayama, Y. (1996). *J. Electrochem. Soc.* **143**, 2670–2673.
Montes, P. J. & Valerio, M. E. (2010). *J. Lumin.* **130**, 1525–1530.
Moreau, G., Helm, L., Purans, J., Merbach, A. E. (2002*a*). *J. Phys. Chem. A*, **106**, 3034–3043.
Moreau, G., Scopelliti, R., Helm, L., Purans, J., Merbach, A. E. (2002*b*). *J. Phys. Chem. A*, **106**, 9612–9622.
Ohta, M., Maruyama, M., Hayakawa, T. & Nishijo, T. (2000). *J. Ceram. Soc. Jpn*, **108**, 284–289.
Pei, Z. W., Su, Q. & Zeng, Q. H. (1996). *Chin. J. Lumin.* **17**, 114.
Peng, M., Pei, Z., Hong, G. & Su, Q. (2003). *J. Mater. Chem.* **13**, 1202–1205.
Ravichandran, D., Roy, R., White, W. B. & Erdei, S. (1997). *J. Mater. Res.* **12**, 819–824.
Rezende, M. S., Montes, P. J., Valerio, M. E. & Jackson, R. A. (2012). *Opt. Mater.* **34**, 1434–1439.
Rodrigues, A. R. D., Craievich, A. F. & Gonçalves da Silva, C. E. T. (1998). *J. Synchrotron Rad.* **5**, 1157–1161.
Takeyama, T., Nakamura, T., Takahashi, N. & Ohta, M. (2004). *Solid State Sci.* **6**, 345–348.
Wortmann, G. (1989). *Hyperfine Interact.* **47**, 179–202.
Yokota, K., Zhang, S. X. & Kimura, K. (2001). *J. Lumin.* **92**, 223.
Zeng, Q. H., Pei, Z. W., Wang, S. B. & Su, Q. (1998). *J. Alloy. Compd.* **275**, 238–241.
Zhang, J., Zhang, Z., Tang, Z., Tao, Y. & Long, X. (2002). *Chem. Mater.* **14**, 3005–3008.